Earth and Planetary Science Letters
October 2014, Volume 404, Pages 376–388
http://dx.doi.org/10.1016/j.epsl.2014.08.014

Trace element behaviour at cold seeps and the potential export of dissolved iron to the ocean

Nolwenn Lemaitre[a, b, c], Germain Bayon[a, *], Hélène Ondréas[a], Jean-Claude Caprais[d], Nicolas Freslon[a, b], Claire Bollinger[b, c], Marie-Laure Rouget[b, c], Alexis de Prunelé[a, b], Livio Ruffine[a], Karine Olu-Le Roy[d], Géraldine Sarthou[b, e]

[a] IFREMER, Unité de Recherche Géosciences Marines, F-29280 Plouzané, France
[b] UEB, Université Européenne de Bretagne, F-35000 Rennes, France
[c] IUEM, Institut Universitaire Européen de la Mer, Université de Bretagne Occidentale, CNRS UMS 3113, IUEM, F-29280 Plouzané, France
[d] IFREMER, Unité de Recherche Etudes des Ecosystèmes Profonds, F-29280 Plouzané, France
[e] LEMAR, UMR 6539, CNRS, Université de Brest, IRD, Ifremer, IUEM, F-29280 Plouzané, France

*: Corresponding author : Nolwenn Lemaitre, tel.: +33 2 98 22 46 30 ; email address : gbayon@ifremer.fr

Abstract:

Seawater samples were collected by submersible above methane seeps in the Gulf of Guinea (Regab and Baboon pockmarks) in order to investigate the behaviour of iron (Fe), manganese (Mn) and rare earth elements (REE) during fluid seepage. Our aim was to determine whether cold seeps may represent potential sources of dissolved chemical species to the ocean. Dissolved (<0.45 µm filtered samples) and total dissolvable (unfiltered samples) concentrations were determined over ~50 m long vertical transects above the seafloor and at various discrete locations within the pockmarks.

We show that substantial amounts of Fe and Mn are released into seawater during seepage of methane-rich fluids. Mn is exported almost quantitatively in the dissolved form (more than 90% of total Mn; mean Mn_{DISS}~12±11 nmol/kg~12±11 nmol/kg). Although a significant fraction of Fe is bound to particulate phases, the dissolved iron pool still accounts on average for approximately 20 percent of total iron flux at vent sites (mean Fe_{DISS}~22±11 nmol/kg~22±11 nmol/kg). This dissolved Fe fraction also appears to remain stable in the water column. In contrast, there was no evidence for any significant benthic fluxes of pore water REE associated with fluid seepage at the studied sites.

Overall, our results point towards distinct trace element behaviour during fluid seepage, with potential implications for the marine geochemical budget. The absence of any dissolved REE enrichments in bottom waters clearly indicates effective removal in sub-surface sediments. Most likely, precipitation of authigenic mineral phases at cold seeps (i.e. carbonates) represents a net sink for these elements. While Mn appears to behave near-conservatively during fluid seepage, the observed relative stability of dissolved Fe in the water column above seepage sites could be explained by complexation with strong organic ligands and/or the presence of Fe-bearing sulfide nanoparticles, as reported previously for submarine hydrothermal systems. Considering the ubiquitous occurrence of methane vents at ocean margins, cold seeps could represent a previously unsuspected source of dissolved Fe to the deep ocean.

Highlights

► Large amounts of dissolved Fe and Mn are released into seawater at methane seeps. ► Possible role of organic complexation or sulfide nanoparticles in stabilizing Fe. ► Cold seeps could represent an important source of dissolved Fe to the deep ocean. ► Precipitation of authigenic minerals leads to removal of REE in sediments.

Keywords: iron ; rare earth elements ; cold seeps ; seawater ; organic ligands ; iron-sulfide nanoparticles

1 - Introduction

At ocean margins, the progressive accumulation of organic-rich sediments on the seafloor leads, with time and microbial degradation, to diagenetic remineralization of organic compounds and to methanogenesis (e.g. Martens and Berner, 1974). The migration of methane-rich fluids in sediment and subsequent release into bottom waters typically result in the formation of venting structures, such as pockmarks or mud volcanoes (e.g. Suess, 2010). These so-called 'cold' seeps are particularly common at margins, and hence could play an important role in the exchange processes between seawater and sediment, and in the distribution of trace elements in the water column.

Fluid venting at cold seeps sustains the development of abundant seafloor ecosystems, which rely on the chemosynthetic use of reduced chemical compounds (e.g. Sibuet et al., 1998). The main biogeochemical process in fluid venting areas is the anaerobic oxidation of methane (AOM). The AOM is generally coupled with sulfate reduction in anoxic sediments, which are both driven by microbial assemblages of archaea and bacteria, respectively (e.g. Boetius et al., 2000). This results in the release of bicarbonate ions and hydrogen sulfide into pore waters, which, in turn, often leads to precipitation of authigenic minerals, such as carbonates and sulfides (e.g. Aloisi et al., 2002).

Both microbial activity and carbonate precipitation represent a net sink for methane at cold seeps (e.g. Luff and Wallmann, 2003; Boetius and Wenzhofer, 2013). However, in highly active environments, excess methane can be expelled into bottom waters. Methane plumes can rise up to several kilometers through the water column, as inferred from direct CH_4 measurements and acoustic investigations of gas flares at margins worldwide (Charlou et al., 2003; Charlou et al., 2004; Sauter et al., 2006; Greinert et al., 2006; Mastalerz et al., 2007; Solomon et al., 2009; Westbrook et al., 2009; Brothers et al., 2013; Kannberg et al., 2013). The emission of methane-rich fluids at the seafloor is also typically associated with high particulate contents, which can be detected using nephelometers and/or measurements of high concentrations of Fe and Mn in seawater (e.g. Charlou et al., 2004; Sauter et al., 2006; Bayon et al., 2011a). By analogy with submarine hydrothermal systems, it is generally assumed that the mixing of anoxic fluids with oxygen-rich bottom waters leads to the precipitation of Fe and Mn oxyhydroxides in methane plumes (Charlou et al., 2004; Bayon et al., 2011a). However, with the exception of barium (Kasten and Jorgensen, 2000; Dickens, 2001; Torres et al., 2002; Aloisi et al., 2004; Riedinger et al., 2006; McQuay et al., 2008; Kasten et al.,

2012; Griffith and Paytan, 2012), the behaviour of iron, manganese and other trace elements during fluid seepage remains largely unexplored. In particular, it is unknown whether cold seeps may represent, or not, a source of dissolved iron to seawater.

Most dissolved iron in seawater is complexed with natural organic ligands (e.g. Rue and Bruland, 1995; Laglera and van den Berg, 2009; Gledhill and Buck, 2012; Misumi et al., 2013). Iron-organic complexes are characterized by high stability constants in the marine environment, which prevents (or delays) precipitation and enhances dissolved Fe concentrations in seawater (e.g. Sander and Koschinsky, 2011; Gledhill and Buck, 2012). Over recent years, several studies have demonstrated the presence of Fe-binding organic complexes in hydrothermal fluids and plumes, with global implications for the global Fe budget (Sander et al., 2007 & 2011, Bennett et al., 2008; Toner et al., 2009; Tagliabue et al., 2010; Wang et al., 2012; Hawkes et al., 2013; Saito et al., 2013). The hypothesis that reduced iron species could leak from hydrothermal vents was also suggested by speciation studies of plume particles, revealing the presence of non-sulfide iron(II) phases associated with carbon-rich material (Statham et al., 2005; Toner et al., 2009; Toner et al., 2012). In addition, Fe-bearing sulfide nanoparticles are also typically present within hydrothermal plumes (Yücel et al., 2011; Gartman et al., 2014). Because nanoparticulate sulfides are not retained onto filters with a 0.45µm or 0.22µm pore size filters, they have been shown to account for a significant fraction (as high as 25 wt%) of the so-called 'dissolved' iron at hydrothermal vents (Yücel et al., 2011; Gartman et al., 2014). At present, the fate of these very fine sulfide particles within methane plumes is unknown, but they could possibly be transported over long distances in the deep ocean (Carazzo et al., 2013).

The main objective of this study was to investigate the behaviour of iron and manganese at cold seeps, and to assess the potential significance of fluid seepage to the global oceanic budget. The work presented here focused on methane seeps from the Gulf of Guinea, including the Regab pockmark, a well-studied highly active seepage site on the Congo margin (Ondréas et al., 2005). In addition to Fe and Mn, we also used the rare earth elements (REE), because their behaviour at cold seeps is presumably related to Fe and Mn cycling (Bayon et al., 2011). The REE also represent potentially interesting tracers of fluid seepage at margins, because they are generally highly enriched in pore waters relative to overlying bottom waters (Haley et al., 2004). A study conducted above methane seeps at the Niger delta margin suggested however that REE could be quantitatively scavenged during fluid emission,

presumably due to scavenging onto Fe-Mn oxyhydroxide phases in sub-surface sediments (Bayon et al., 2011a).

2 – Study area

In the Gulf of Guinea, the Congo margin is the location of several active sites of venting fluid (Ondréas et al., 2005; Sahling et al., 2008; Pierre et al., 2012). The most studied site in this area is Regab, a giant pockmark of about 800m wide, located at 3160m depth near the Congo submarine canyon (Fig. 1). This canyon has been directly connected to the mouth of the Congo River, at least since the Quaternary period, thereby acting as a direct source-to-sink route for sediments from the continent to the deep sea basin (Babonneau et al., 2002). It delivers substantial amounts of organic-rich sediments to the entire Congo submarine system (Baudin et al., 2010). Regab was first explored during the Zaiango project (1998-2000), and was further investigated during subsequent cruises (e.g., Ondreas et al., 2005; Pop-Ristova et al., 2012). The source of methane-rich fluids at Regab is thought to derive from a buried palaeo-channel of the Congo River (Ondréas et al., 2005). Regab is characterized by intense methane seepage and the occurrence of gas hydrates, massive carbonate deposits, and abundant chemosynthetic communities at the seafloor (Ondréas et al., 2005; Charlou et al., 2004; Gay et al., 2006; Pierre and Fouquet, 2007; Olu-LeRoy et al., 2007; Olu et al., 2009; Marcon et al., 2014a; Duperron et al., 2014). Over recent years, several other active venting sites, known as the Kouilou pockmarks, have also been discovered on the northern Congo margin, about 100 km north of Regab (Sahling et al., 2008; Pierre et al., 2012). This includes the Baboon pockmark (~ 3000 m depth), characterized like Regab by the occurrence of gas hydrate deposits, seafloor carbonate pavements, and intense methane seepage.

3 – Materials and methods

3.1. Microbathymetric map, seafloor observations and sampling

The seafloor photographs and microbathymetric data presented in this study were acquired via the Victor 6000 ROV (Remote Operated Vehicle) during the WACS expedition (2011) aboard R/V *Pourquoi Pas?* (chief scientist: K. Olu-Le Roy). The new microbathymetric data provide details of seafloor morphology at Regab with an unprecedented high-resolution (Marcon et

al., 2014b). Seafloor submersible observations are superimposed onto the new microbathymetric map in Fig. 2. The central part of the pockmark is composed of several large clustered depressions (about 50 m wide), where the most active seepage sites are concentrated (Ondréas et al., 2005; Marcon et al., 2014b). This area is characterized by seafloor occurrence of gas hydrates and carbonate crusts, active gas plumes, and dense mussel (*Mytilidae*) and clam (*Vesicomyidae*) beds (Fig. 3a,b,c,d). The northern part of Regab also displays a rough topography with irregular outcrops of carbonate crusts serving as hard substrates for dense bushes of vestimentiferan (*Escarpia southwardae*) tubeworms (Fig. 3e). In contrast, the western and southern parts of the pockmark are mainly composed of bioturbated sediment riddled with small meter-wide holes. In this area, a few larger depressions (about 10 m wide) are often found in association with patches of clams (Vesicomyidae) and microbial mats related to reduced sediments (Fig. 3f).

Seawater samples were collected using the automated PEPS system, which allowed sampling of twelve individual acid-cleaned 2L plastic bags during each ROV dive (Table 1). At Regab, the seawater samples were taken along vertical profiles up to about +60 m above the seafloor at three different stations: 1) a highly active site of gas venting in the center of the pockmark (hereafter referred to as the 'Bubble' site); 2) another active area in the eastern part of the pockmark (i.e. East Pockmark site), at about 300 m from the Bubble Site; and 3) a reference station (i.e. Reference site), also located eastwards at about 1 km away from the center of the pockmark (Fig. 2). These sampling sites were selected based on results from a previous ROV survey, during which bottom water samples were collected and further analysed for methane concentrations (Charlou et al., 2004; Fig. 2). The methane contents measured at these three sites were ~ 130 µl/l, 17 µl/l and 0.05 µl/l, respectively (Charlou et al., 2004; Table S1). While the bottom water sample at the reference site was characterized by much lower CH_4 contents, this value was still significantly higher than typical deep water methane background levels in the Atlantic Ocean (6-8 nl/l; Lamontagne et al., 1973), suggesting that this location was also under the influence of methane plumes from Regab. During the WACS expedition, seawater was also collected at just a few centimeters above the seafloor within the pockmark, next to patches of vesicomyid clams, mussels (two sites) and microbial mats. At Baboon, samples were collected at 3 m above the seafloor during a ROV dive across the pockmark. All samples were filtered on board onto <0.45 µm cellulose filters within a few hours after collection. Both filtered and unfiltered samples were directly transferred into acid-cleaned

157 HDPE Nalgene® bottles, and further acidified on board with twice sub-boiled nitric acid to
158 pH ~ 2.

159

160 **3.2. Chemical and analytical procedures**

161 The bottom water samples collected at Baboon and above the seafloor chemosynthetic
162 habitats investigated at Regab were analysed for methane concentrations. On board, 5-ml
163 seawater aliquots were conditioned into 10-ml serum vials, poisoned with 20µl $HgCl_2$, and
164 stored at 4°C. Methane concentrations were then determined onshore by static headspace gas
165 chromatography (Perichrom® Pr2100). The chemical preparations prior to trace element
166 measurements were conducted back to the clean laboratory (ISO-6) at Brest. All experiments
167 were made in polypropylene tubes cleaned with the following sequence: 5% nitric acid, milli-
168 Q 18.2MΩ water, 2% nitric acid twice sub-boiled and milli-Q 18.2MΩ water. Pipette tips
169 used for the experiments underwent the same cleaning procedure. All measurements were
170 made using mass spectrometry techniques at the Pôle Spectrométrie Océan (PSO, Brest).

171 Rare earth elements, Y, Fe, and Mn concentrations were determined by sector field ICPMS
172 (Element2) after addition of mixed ^{57}Fe-thulium (Tm) spike and double magnesium
173 ($Mg(OH)_2$) co-precipitation (Wu, 2007; Freslon et al., 2011). The iron concentration of the
174 spike was calibrated by inverse isotopic dilution using several certified reference geological
175 materials (MGL-AND, BIR-1, BCR-1, HTB-1). The $Mg(OH)_2$ co-precipitation was
176 performed on carefully weighed seawater samples (about 25 ml) by adding ultra-pure
177 ammonia (Optima, Fisher Scientist, VWR BDH Prolabo, 25%). After two successive co-
178 precipitations, the final $Mg(OH)_2$ precipitate was cleaned and further dissolved in 2% Ultrex®
179 II HNO_3 prior to ICPMS analysis. Measured REE concentrations were corrected for oxide
180 and hydroxide interferences (Barrat et al., 1996). Iron and Mn counts were measured in the
181 medium resolution mode of the Element2 SF-ICPMS. Iron concentrations were determined
182 by isotopic dilution, while the abundances for other elements (Mn, REE, Y) were calculated
183 using the Tm addition method (Bayon et al., 2011b; Freslon et al., 2011).

184 Procedural blanks for all studied elements were determined using the same methods as for
185 water samples, applied to a seawater sample depleted in trace elements by five successive
186 magnesium co-precipitations. Total blank contributions for Fe (1.4 ± 0.5 ng; N=12; 1SD)
187 were always below 20% in our samples. Average blank contributions for all other elements

were generally negligible. The accuracy and precision of our analyses were assessed using two certified reference materials (NASS-6 and CASS-5), and one in-house seawater standard (Concarneau Bay, Brittany, France). Replicate analyses of the two certified seawater standards gave accuracies better than 7% for Fe and Mn compared to certified values (Table S1). The corresponding relative standard deviations (RSD%) were lower than 33% for Mn and Fe (Table S2). For REE and Y, both accuracies (for CASS-5; Rousseau et al., 2013) and precisions were generally better than 8%, with the exception of Yttrium (Y, RSD <13%), Lanthanum (La, RSD <13%), and Cerium (Ce, <25%). As will be discussed below, all studied samples were characterized by REE shape patterns typical of seawater and/or Fe-Mn oxyhydroxide phases. One unfiltered sample however (Bubble site +5 m; Table 2) displayed anomalously high La and Ce concentrations, perhaps due to contamination, and hence was discarded in the following discussion.

4 – Results

The bottom waters sampled above the seafloor habitat patches at Regab (+ 0.1m) and at Baboon (+ 3m) exhibit high CH_4 concentrations, ranging between ~ 32-132 µl/l and 10-70 µl/l, respectively (Table S2). Vertical profiles for dissolved (filtered samples) and total dissolvable (unfiltered samples) element concentrations at the three studied Regab stations are shown in Fig. 4. The corresponding data are listed in Table 2 and Table 3. The Bubble station is characterized by marked enrichments of iron and manganese in unfiltered seawater samples (up to ~400 and ~20 nmol/kg, respectively), which are clearly related to emission of methane-rich fluids in the central part of Regab (Fig. 2). An important feature is that bottom waters also retain elevated concentrations of both dissolved Fe and Mn, at least as high as +40 m above the seafloor (about ~30-40 and ~12-20 nmol/kg, respectively). Seafloor samples collected above chemosynthetic habitats at Regab and across the Baboon pockmark display similar concentration levels (Fe_{DISS} ~7-34 nmol/kg and Mn_{DISS} ~3-47 nmol/kg). In comparison, the bottom water column at the Reference site exhibits lower values, with Fe_{DISS} ~5-10 nmol/kg and Mn_{DISS} ~5-8 nmol/kg (when excluding the sample nearest to the seafloor, Mn_{DISS} ~19 nmol/kg). Although this latter station is located at about 1 km away from the Regab center, it has to be noted however that these 'reference' Fe_{DISS} and Mn_{DISS} values are still much higher than typical open-ocean deep water values in the South Atlantic (i.e. < 0.7 nmol/kg; Noble et al., 2012).

Rare earth element concentrations in unfiltered samples are generally higher near the seafloor (up to TDNd ~ 80 pmol/kg). Measured dissolved REE concentrations range from e.g. Nd_{DISS} ~ 20 to 42 pmol/kg. The lowest Nd_{DISS} concentrations were determined in the water column overlying the Bubble site (mean value of ~ 21.6 ± 1.6 pmol/kg). In comparison, dissolved REE concentrations in the bottom water column at the Reference station are higher (mean Nd_{DISS} ~ 26 ± 1 pmol/kg). With one exception, all seawater samples from the reference site exhibit very similar seawater-like REE patterns (e.g. Elderfield and Greaves, 1982), showing a pronounced negative Ce-anomaly and a progressive enrichment from the light- (LREE) to the heavy-REE (HREE) (Fig. 5). In contrast, a few unfiltered samples from the Bubble Site (+1 m), the Reference Site (+1m), and seafloor habitat patches display much higher REE concentrations and a distinctive shale-normalized REE pattern, with a less negative (or positive) Ce-anomaly and mid-REE (MREE) enrichment over HREE (Fig. 5).

5 – Discussion

5.1. Evidence for a decoupling between REE and Fe

The distribution patterns of rare earth elements provide useful information on both fluid sources and the origin of particulate phases at submarine hydrothermal vents and cold seeps (e.g. German et al., 1990; Sherrell et al., 1999; German et al., 2002; Edmonds and German, 2004; Bayon et al., 2011a). At the Reference site, the REE pattern shape of the unfiltered sample collected at +1 m over the seafloor is characteristic of the Fe-Mn oxyhydroxide fraction that can be extracted from marine sediments by sequential leaching, including those from the Gulf of Guinea (Bayon et al., 2004; Bayon et al., 2011a). Considering that high TDFe and TDMn concentrations were also found in the same sample, this indicates that high particulate load is probably present in seawater at this location. By analogy, a similar conclusion can also be drawn from the REE pattern shapes determined for other unfiltered seawater samples at Baboon and over seafloor habitat patches and the Bubble vent site (+ 1m) at Regab (Fig. 5). Such TDREE, Mn, Fe enrichments in bottom waters overlying active seepage sites are clearly diagnostic of sediment resuspension due to emission of gas-rich fluids at submarine vents, similar to what has been previously proposed (Charlou et al., 2004; Bayon et al., 2011a). On the Niger Delta margin, this is nicely illustrated by the positive correlation displayed by TDFe and TDNd in seawater samples collected above active pockmarks and mud volcanoes (Fig. 6).

Interestingly, however, Fe and REE appear to behave slightly differently in the water column at the Regab and Baboon pockmarks (Fig. 6). While bottom waters at the Bubble site and Baboon display a large range of TDFe values (between ~70 to 600 nmol/kg), generally much higher than those for the Reference and East Pockmark stations (between ~30 to 60 nmol/kg), TDNd yields similar levels of concentrations in most samples. This is clearly shown on the TDNd versus TDFe plot (Fig. 6), suggesting that Fe and REE are decoupled during fluid venting at Regab.

One possible explanation accounting for the observed decoupling between Fe and REE would be that TDFe is not solely controlled by Fe-oxyhydroxide phases in methane plumes. At hydrothermal vents, the iron budget in plume particles is dominated by Fe-oxyhydroxide/oxide phases, but also by Fe-sulfide minerals (e.g. Toner et al., 2009; Breier et al., 2012). Iron speciation measurements have shown that oxidized iron(III) and sulfides could account for about 10 mol% and ~ 60-70 mol% of total iron in hydrothermal plume particles, respectively (Toner et al., 2009; Toner et al., 2012). Iron sulfides precipitate within the buoyant plumes, immediately after hydrothermal discharge into the water column. Then, the increase of pH and dissolved O_2 contents in the non-buoyant plume usually leads to precipitation of the remaining (or most of it) dissolved iron as Fe-oxyhydroxides. Like hydrothermal systems, cold seeps are also generally characterized by high sulfide concentrations (up to ~ 10 mM in pore waters at Regab; Pop-Ristova et al., 2012). It seems unlikely that acidification to pH ~ 2 would achieve complete dissolution of Fe-sulfide phases in our unfiltered samples. However, because REE are strongly depleted in sulfide minerals (e.g. Tachikawa et al., 2013), only partial dissolution of particulate Fe-sulfide phases in bottom waters at the Bubble site could perhaps explain the observed decoupling between Fe and REE. The distinct TDFe vs. TDNd trends that can be inferred from the Regab and Baboon data in Fig. 6 could hence be possibly explained by a combination of both sulfide and oxyhydroxide precipitation. At the Niger seeps, seawater samples were collected by a CTD/Rosette system operated from the deck, suggesting that they may not be representative of the methane plumes expelled immediately above venting sites. This is also suggested by the fact that the Niger samples are characterized by relatively low methane contents (i.e. about one order of magnitude lower) compared to those collected by ROV above the Congo seeps. The absence of any sulfide enrichment in the Niger samples could hence suggest that these particles are not efficiently transported over long distances in deep waters.

In addition, removal of substantial amounts of dissolved REE from pore waters before seafloor venting of methane-rich fluids could also potentially contribute to the observed decoupling between Fe and REE at Regab. At cold seeps, precipitation of authigenic carbonate minerals (e.g. aragonite, high-Mg calcite) commonly takes place in anoxic sub-surface sediments or bottom waters, in relation to anaerobic oxidation of methane (e.g. Aloisi et al., 2002; Bayon et al., 2013). The high REE contents determined in methane-derived carbonates suggest that carbonate precipitation probably represents an important sink for REE in marine sediments (Himmler et al., 2010; Rongemaille et al., 2011; Feng et al., 2013). This has been recently confirmed in a study reporting pore water REE data at Hydrate Ridge (NE Pacific Ocean), which showed that REE were almost quantitatively depleted at the sulfate-methane interface (Himmler et al., 2013). In areas characterized by high methane fluxes, such as the central part of Regab (Pop-Ristova et al., 2012), both AOM and carbonate precipitation takes place at only a few centimeters below the seafloor. As a consequence, intense carbonate precipitation could possibly influence, at least locally, REE distribution in bottom waters, thereby perhaps explaining the slightly lower dissolved REE concentrations at the Bubble site (mean Nd_{DISS} ~ 21.6 ± 1.6 pmol/kg) compared to the Reference station (mean ~ 26 ± 1 pmol/kg).

Overall, our data for unfiltered seawater samples hence suggest that REE and Fe are decoupled during fluid venting at cold seeps, due to the combined precipitation of both REE-rich Fe-oxyhydroxide and REE-poor Fe-sulfide phases in the methane plumes, but also possibly in sub-surface sediments, during precipitation of authigenic carbonate deposits.

5.2. The distribution of dissolved Fe and Mn in the water column

The observed positive correlations between CH_4, and Fe_{DISS} and Mn_{DISS} concentrations in the studied seawater samples clearly show that fluid seepage at Regab and Baboon is accompanied with substantial release of dissolved iron and manganese species (Fig. 7). Over the last decades, a large amount of work has been conducted on submarine hydrothermal plumes, which provides useful background information for predicting trace element behaviour at cold seeps. Dissolved Mn is known to oxidize very slowly in hydrothermal plumes, exhibiting near-conservative behaviour on time scales of days to weeks (e.g. Cowen et al., 1990). At the Congo seeps, both unfiltered and filtered seawater samples generally display very similar Mn concentrations (within 20% in most cases), including above the active

316 Bubble vent site. This indicates that Mn is mainly present in soluble form, remaining stable at
317 least over the time scale of the age of the plumes sampled at Regab. At the Bubble site, the
318 highest dissolved Mn concentrations (Mn_{DISS} ~21 nmol/kg) were determined at about +40 m
319 above the seafloor (Fig. 4), possibly indicating the presence of another discrete plume in the
320 water column. This result would be in agreement with evidence from the CH_4 distribution
321 map above the seafloor at Regab (Charlou et al., 2004; Fig. 5), which clearly suggests that
322 distinct methane plumes may co-exist in the water column, especially in the central part of the
323 pockmark.

324 In contrast to Mn, iron oxidation rates reported at hydrothermal sites are much higher (Millero
325 et al., 1987; Millero et al., 1998; Field and Sherrell, 2000; Statham et al., 2005). Dissolved
326 iron generally oxidizes within minutes or hours in seawater and non-buoyant plumes,
327 depending on bottom water chemistry (pH, O_2 and H_2O_2 contents; Gonzalez-Davila et al.,
328 2006; Sarthou et al., 2011). The same process probably explains the large differences
329 observed between measured TDFe (higher) and Fe_{DISS} (lower) concentrations at Regab (Fig.
330 4; Table 2), implying that a substantial amount of released iron is associated with particulate
331 oxyhydroxide and/or sulfide phases (i.e. see section 5.2). At the active Bubble site, however,
332 the dissolved Fe pool accounts for a non-negligible 22 ± 7 % of total iron in the water column.
333 Interestingly, while TDFe values markedly decrease from seafloor to +20 m height (from ~
334 400 to 100 nmol/kg; Table 2), dissolved Fe concentrations remain at relatively similar levels
335 (Fe_{DISS} ~ 33 ± 5 nmol/kg). Moreover, considering that the plume sampled at +40 m is older
336 than near-seafloor fluids collected just above the vent, another striking feature of our data is
337 evidence that seawater samples collected at both +1 m and +40 m exhibit very similar
338 dissolved Mn/Fe ratio (~ 0.4-0.6).

339 At Regab, the theoretical dissolved Fe(II) oxidation rate predicted using the approach
340 developed by Millero et al. (1987) gives an oxidation half-life for iron of about 40 min. This
341 calculation is made using well-constrained temperature (T = 2.4°C), pH (7.8), and O_2 (240
342 mM) bottom water conditions (Charlou et al., 2004; Olu et al., 2007). In agreement with the
343 relatively high methane concentration measured at the Reference site (46 nl/l; Charlou et al.,
344 2004), the high Fe_{DISS} concentrations determined in the bottom water column at the same
345 location suggest that this site is still under the influence of Regab methane plumes. The
346 residual deep currents in the Regab area, averaged over a one-year period, are oriented
347 eastward with a mean speed of 4.1 cm/s (Vangrieshiem et al., 2009), and hence would be
348 likely to transport methane-rich fluids from Regab to the Reference site. As opposed to

hydrothermal vents, fluid escape at cold seeps is not restricted to localized discharge sites only, so that it is difficult to infer the source of Fe and Mn at the Reference station. However, considering the distance between the Regab center and the Reference station (about 1 km), a minimum advection time of about 7 hours can be calculated, which is long compared to the theoretical Fe oxidation half-life (~ 40 min). Using this theoretical value, the measured dissolved Fe concentrations at the Reference site would correspond to an advection time of 45 min, which would hence require an unlikely bottom current speed of ~ 37 cm/s. Therefore, and although a substantial amount of iron emitted at the Congo seeps appears to be linked to particulate phases, all the above consideration suggests that Fe(II) oxidation rates in bottom waters are longer than theoretical rates. This implies that a dissolved iron fraction probably remains relatively stable above the pockmark after emission into the water column, which is then likely to be further transported away with bottom currents.

5.3. The stabilization of dissolved iron at cold seeps – possible implication for the global iron budget in the ocean

As discussed above, a substantial fraction of the dissolved iron released at the Baboon and Regab pockmarks is probably stabilized in bottom waters. By analogy with submarine hydrothermal vents, the high concentrations and apparent stability of dissolved iron at the Congo seeps could be explained by complexation onto organic ligands (e.g. Bennett et al., 2008; Toner et al., 2009; Sander and Koschinsky, 2011) and/or the presence of sulfide nanoparticles (Yücel et al., 2011; Gartman et al., 2014).

On margins, methane seepage and associated biogeochemical processes are intimately linked to organic matter recycling. In sub-surface sediments, early diagenetic processes typically release hydrolysable compounds into pore waters, such as amino acids and fatty acids (e.g. Chester and Jickells, 2012). Under anoxic conditions, further degradation of organic compounds can also cause substantial enrichments in dissolved humic substances (Wallmann et al., 2008). Because high rates of organic matter deposition occur typically on ocean margins, cold seeps could clearly represent a plentiful supply of metal-binding organic ligands. At submarine hydrothermal systems, the amount of stabilized Fe(II) and Fe(III) is expected to be controlled to some extent by the availability of dissolved organic ligands in methane plumes (e.g. Bennett et al., 2008). Considering the eventuality that methane-rich fluids at cold seeps may be more enriched in organic ligands than their analogs from mid-

ocean ridges, this would also imply that they may have the capacity to sustain higher amounts of organically-bound dissolved Fe.

Continental margins had already been identified as important sources of dissolved iron to seawater, especially at oxygen minimum zones (Bruland et al., 2005; Noble et al., 2012). Elrod et al. (2004) even argued that the input of dissolved Fe from continental shelves could be as significant as the global iron input from aerosols. The present study suggests for the first time that methane venting at margins worldwide could also represent a source of dissolved Fe to seawater. To the best of our knowledge, there are unfortunately no other published data for dissolved iron and ligand concentrations in seawater at cold seeps that would enable us to quantify the contribution of cold seep iron to the global ocean budget. Based on our results, a first tentative estimate may be derived using the correlation observed between CH_4 and dissolved Fe concentrations at the Congo seeps. The latest global estimate of methane efflux from submarine seeps to the overlying ocean is about 0.02 Gt of carbon annually (Boetius and Wenzhöfer, 2013), which corresponds to the export of ~ 2.2 x 10^{12} moles of CH_4 per year. This estimate is based on the presumption that a few tens of thousands of colds eeps are active at ocean margins worldwide (Boetius and Wenzhöfer, 2013). Assuming that a simple linear regression ($[Fe_{DISS}] = 0.0038 \times [CH_4]$; Fig. 7) characterized the global relationship between CH_4 and Fe_{DISS} emitted at seeps, we can calculate an annual dissolved iron flux of ~ 8.4 x 10^9 moles. Of course, a substantial fraction of this estimated dissolved iron flux probably includes inorganic colloids and nano-sulfide particles that are not retained onto 0.45 μm or 0.2 μm filters, but would remain in the so-called dissolved phase for presumably a limited time only. At hydrothermal vents, about 30% of the total dissolved iron in plumes is bound to ligand phases and is truly available as a labile form to the deep ocean (Hawkes et al., 2013). Assuming that a similar percentage also applies to cold seep settings, we can estimate a dissolved iron flux of about 2.5 x 10^9 moles per year. While this first-estimate value should be taken with great caution, as it is probably associated with large uncertainty, it would be roughly similar to the dissolved iron inputs calculated for hydrothermal vents (from ~ 3 x 10^8 to 1.5 x 10^9 mol/yr; Bennett et al., 2008; Tagliabue et al., 2010; Carazzo et al., 2013). This would imply that cold seeps, like submarine hydrothermal systems, potentially represent a substantial source of dissolved iron to the deep ocean.

6- Conclusion

The data presented in this study confirm that precipitation of authigenic minerals probably represents a net sink for rare earth elements at seeps from the Congo margin. The formation of carbonate crusts/concretions in sub-surface sediments most likely prevents emission of dissolved REE and Ba into the overlying water column. In contrast, we show for the first time that substantial amounts of dissolved iron and manganese can be released into bottom waters at methane seeps. A significant fraction of Fe within methane plumes is present in the particulate fraction, probably in association with both Fe-Mn oxyhydroxides and sulfide mineral phases. Importantly, the dissolved Fe fraction released at vent sites appears to remain relatively stable in the water column, due possibly to iron complexation with strong organic which prevents Fe co-precipitation into mineral phases. To some extent, the presence of Fe-bearing sulfide nanoparticulates in methane plumes could also account for the high concentrations and apparent stability of dissolved iron in bottom waters. These results suggest that seepage of methane-rich fluids at margins could be accompanied by substantial export of dissolved Fe to seawater, with possible implications for the global dissolved iron budget in the deep-ocean. To test these hypotheses, future studies should aim at characterizing iron speciation in methane plumes on ocean margins, and further quantify dissolved Fe fluxes at cold seeps.

Acknowledgements

We thank the Captain, the crews and all scientific participants onboard the R/V *Pourquoi Pas?* during the WACS expedition. In particular, C. Le Gall is warmly thanked for assistance at sea for handling the PEPS seawater sampling system. We also acknowledge J. Etoubleau, D. Birot, and Y. Germain for assistance in the laboratory; and A.-S Alix and M. Guillou for their help in GIS at IFREMER. Finally, the editor, Gideon Henderson, and four anonymous reviewers are greatly acknowledged for providing thorough and constructive reviews, which significantly improved an earlier version of this manuscript. This study was funded by IFREMER.

443 **References**

444 Aloisi, G., Bouloubassi, I., Heijs, S.K., Pancost, R.D., Pierre, C., Damste, J.S.S., Gottschal,
445 J.C., Forney, L.J., Rouchy, J.M., 2002. CH4-consuming microorganisms and the
446 formation of carbonate crusts at cold seeps. Earth Planet. Sci. Lett. 203, 195-203.

447 Aloisi, G., Wallmann, K., Bollwerk, S.M., Derkachev, A., Bohrmann, G., Suess, E., 2004.
448 The effect of dissolved barium on biogeochemical processes at cold seeps. Geochim.
449 Cosmochim. Acta 68, 1735-1748.

450 Babonneau, N., Savoye, B., Cremer, M., Klein, B., 2002. Morphology and architecture of the
451 present canyon and channel system of the Zaire deep-sea fan. Mar. Petrol. Geol. 19, 445-
452 467.

453 Barrat, J.A., Keller, F., Amosse, J., Taylor, R.N., Nesbitt, R.W., Hirata, T., 1996.
454 Determination of rare earth elements in sixteen silicate reference samples by ICP-MS
455 after Tm addition and ion exchange separation. Geostand. Newslett. 20, 133-139.

456 Baudin, F., Disnar, J.R., Martinez, P., Dennielou, B., 2010. Distribution of the organic matter
457 in the channel-levees systems of the Congo mud-rich deep-sea fan (West Africa):
458 Implication for deep offshore petroleum source rocks and global carbon cycle. Mar.
459 Petrol. Geol. 27, 995-1010.

460 Bayon, G., German, C.R., Burton, K.W., Nesbitt, R.W., Rogers, N., 2004. Sedimentary Fe-
461 Mn oxyhydroxides as paleoceanographic archives and the role of aeolian flux in
462 regulating oceanic dissolved REE. Earth Planet. Sci. Lett. 224, 477-492.

463 Bayon, G., Birot, D., Ruffine, L., Caprais, J.C., Ponzevera, E., Bollinger, C., Donval, J.P.,
464 Charlou, J.L., Voisset, M., Grimaud, S., 2011a. Evidence for intense REE scavenging at
465 cold seeps from the Niger Delta margin. Earth Planet. Sci. Lett. 312, 443-452.

466 Bayon, G., Birot, D., Bollinger, C., Barrat, J.A., 2011b. Multi-Element Determination of trace
467 elements in natural water reference materials by ICP-SFMS after Tm Addition and iron
468 co-precipitation. Geostand. Geoanalytical Res. 35, 145-153.

469 Bayon, G., Dupré S., Ponzevera, E., Etoubleau, J., Chéron, S., Pierre, C., Mascle, J., Boetius,
470 A., de Lange G., 2013. Formation of carbonate chimneys in the Mediterranean Sea linked
471 to deep-water oxygen depletion. Nat. Geosci. 6, 755-760.

472 Bennett, S.A., Achterberg, E.P., Connelly, D.P., Statham, P.J., Fones, G.R., German, C.R.,
473 2008. The distribution and stabilisation of dissolved Fe in deep-sea hydrothermal plumes.
474 Earth Planet. Sci. Lett. 270, 157-167.

475 Boetius, A., Wenzhöfer, F., 2013. Seafloor oxygen consumption fuelled by methane from
476 cold seeps. Nat. Geosci. 6, 725-734.

477 Boetius, A., Ravenschlag, K., Schubert, C.J., Rickert, D., Widdel, F., Gieseke, A., Amann, R.,
478 Jorgensen, B.B., Witte, U., Pfannkuche, O., 2000. A marine microbial consortium
479 apparently mediating anaerobic oxidation of methane. Nature 407, 623–626.

480 Breier, J.A., Toner, B.M., Fakra, S.C., Marcus, M.A., White, S.N., Thurnherr, A.M., German,
481 C.R., 2012. Sulfur, sulfides, oxides and organic matter aggregated in submarine
482 hydrothermal plumes at 9 degrees 50 ' N East Pacific Rise. Geochim. Cosmochim. Acta
483 88, 216-236.

484 Brothers, L.L., Van Dover, C.L., German, C.R., Kaiser, C.L., Yoerger, D.R., Ruppel, C.D.,
485 Lobecker, E., Skarke, A.D., Wagner, J.K.S., 2013. Evidence for extensive methane
486 venting on the southeastern U.S. Atlantic margin. Geology 41, 807-810.

487 Bruland, K.W., Rue, E.L., Smith, G.J., DiTullio, G.R., 2005. Iron, macronutrients and diatom
488 blooms in the Peru upwelling regime: brown and blue waters of Peru. Mar. Chem. 93, 81-
489 103.

490 Carazzo, G., Jellinek, A.M., Turchyn, A.V., 2013. The remarkable longevity of submarine
491 plumes: Implications for the hydrothermal inut of iron to the deep-ocean. Earth Planet.
492 Sci. Lett. 382, 66-76.

493 Charlou, J.L., Donval, J.P., Zitter, T., Roy, N., Jean-Baptiste, P., Foucher, J.P., (Foucher, JP);
494 Woodside, J., 2003. Evidence of methane venting and geochemistry of brines on mud
495 volcanoes of the eastern Mediterranean Sea. Deep-Sea Res. I 8, 941-958.

496 Charlou, J.L., Donval, J.P., Fouquet, Y., Ondreas, H., Knoery, J., Cochonat, P., Levache, D.,
497 Poirier, Y., Jean-Baptiste, P., Fourre, E., Chazallon, B., Party, Z.L.S., 2004. Physical and
498 chemical characterization of gas hydrates and associated methane plumes in the Congo-
499 Angola Basin. Chem. Geol. 205, 405-425.

500 Chester, R.R., Jickells, T., 2012. Marine Geochemistry, 3rd Edition. Wiley-Blackwell, Oxford,
501 420pp.

502 Cowen, J.P., Massoth, G.J., Feely, R.A., 1990. Scavenging rates of dissolved manganese in a
503 hydrothermal vent plume. Deep-Sea Res. A 37, 1619-1637.

504 Dickens, G.R., 2001. Sulfate profiles and barium fronts in sediment on the Blake Ridge:
505 Present and past methane fluxes through a large gas hydrate reservoir. Geochim.
506 Cosmochim. Acta 65, 529-543.

507 Duperron, S., Gaudron, S.M., Lemaitre, N., Bayon, G. (2014) Biogeochemical investigation
508 of the cold seep tubeworm Escarpia southwardae (Annelida: Siboglinidae): symbiosis and
509 trace element composition of the tube. Deep-Sea Res. I 90, 105-114.

510 Edmonds, H.N., German, C.R., 2004. Particle geochemistry in the Rainbow hydrothermal
511 plume, Mid-Atlantic Ridge. Geochim. Cosmochim. Acta 68, 759-772.

512 Elderfield, H., Greaves, M.J., 1982. The rare-earth elements in sea-water. Nature 296, 214-
513 219.

514 Elrod, V.A., Berelson, W.M., Coale, K.H., Johnson, K.S., 2004. The flux of iron from
515 continental shelf sediments: A missing source for global budgets. Geophys. Res. Lett. 31,
516 L12307, doi: 10.1029/2004GL020216.

517 Falkner, K.K., Klinkhammer, G.P., Bowers, T.S., Todd, J.F., Lewis, B.L., Landing, W.M.,
518 Edmond, J.M., 1993. The behaviour of barium in anoxic marine waters. Geochim.
519 Cosmochim. Acta 57, 537-554.

520 Feng, D., Lin, Z.J., Bian, Y.Y., Chen, D.F., Peckmann, J., Bohrmann, G., Roberts, H.H.,
521 2013. Rare earth elements of seep carbonates: Indication for redox variations and
522 microbiological processes at modern seep sites. J. Asian Earth Sci. 65, 27-33.

523 Field, M.P., Sherrell, R.M., 2000. Dissolved and particulate Fe in a hydrothermal plume at 9
524 degrees 45 ' N, East Pacific Rise: Slow Fe (II) oxidation kinetics in Pacific plumes.
525 Geochim. Cosmochim. Acta 64, 619-628.

526 Freslon, N., Bayon, G., Birot, D., Bollinger, C., Barrat, J.A., 2011. Determination of rare
527 earth elements and other trace elements (Y, Mn, Co, Cr) in seawater using Tm addition
528 and Mg(OH)(2) co-precipitation. Talanta 85, 582-587.

529 Gartman, A., Findlay, A.J., Luther III, G.W., 2014. Nanoparticulate pyrite and other
530 nanoparticles are a widespread component of hydrothermal vent black smoker emissions.
531 Chem. Geol. 366, 32-41.

532 Gay, A., Lopez, M., Ondreas, H., Charlou, J.L., Sermondadaz, G., Cochonat, P., 2006.
533 Seafloor facies related to upward methane flux within a Giant Pockmark of the Lower
534 Congo Basin. Mar. Geol. 226, 81-95.

535 German, C.R., Klinkhammer, G.P., Edmond, J.M., Mitra, A., Elderfield, H., 1990.
536 Hydrothermal scavenging of rare-earth elements in the ocean. Nature 345, 516-518.

537 German, C.R., Colley, S., Palmer, M.R., Khripounoff, A., Klinkhammer, G.P., 2002.
538 Hydrothermal plume-particle fluxes at 13 degrees N on the East Pacific Rise. Deep-Sea
539 Res. I 49, 1921-1940.

540 Gledhill, M., Buck, K.N., 2012. The organic complexation of iron in the marine environment:
541 A review. Frontiers in Microbiology 3, 1-17, doi: 10.3389/fmicb.2012.00069.

542 González-Dávila, M., Santana-Casiano, J.M., Millero, F.J., 2006. Competition between O2
543 and H2O2 in the oxidation of Fe(II) in natural waters, J. Sol. Chem. 35, 95–111.

544 Greinert, J., Artemov, Y., Egorov, V., De Batist, M., McGinnis, D., 2006. 1300-m-high rising
545 bubbles from mud volcanoes at 2080m in the Black Sea: Hydroacoustic characteristics
546 and temporal variability. Earth Planet. Sci. Lett. 244, 1-15.

547 Griffith, E.M., Paytan, A., 2012. Barite in the ocean - occurrence, geochemistry and
548 palaeoceanographic applications. Sedimentology 59, 1817-1835.

549 Haley, B.A., Klinkhammer, G.P., McManus, J., 2004. Rare earth elements in pore waters of
550 marine sediments. Geochim. Cosmochim. Acta 68, 1265-1279.

551 Hawkes, J.A., Connelly, D.P., Gledhill, M., Achterberg, E.P., 2013. The stabilization and
552 transportation of dissolved iron from high temperature hydrothermal vent systems. Earth
553 Planet. Sci. Lett. 375, 280-290.

554 Himmler, T., Bach, W., Bohrmann, G., Peckmann, J., 2010. Rare earth elements in
555 authigenic methane-seep carbonates as tracers for fluid composition during early
556 diagenesis. Chem. Geol. 277, 126-136.

557 Himmler, T., Haley, B.A., Torres, M.E., Klinkhammer, G.P., Bohrmann, G., Peckmann, J.,
558 2013. Rare earth element geochemistry in cold-seep pore waters of Hydrate Ridge,
559 northeast Pacific Ocean. Geo-Mar. Lett. 33, 369-379.

560 Kannberg, P.K., Trehu, A.M., Pierce, S.D., Paull, C.K., Caress, D.W., 2013. Temporal
561 variation of methane flares in the ocean above Hydrate Ridge, Oregon. Earth Planet. Sci.
562 Lett. 368, 33-42.

563 Kasten, S., Jorgensen, B.B., 2000. Sulfate Reduction in Marine Sediments, in: Schulz, H.D.,
564 Zabel, M. (Eds.), Marine Geochemistry. Springer, New York, pp. 263-282.

565 Kasten, S., Nothen, K., Hensen, C., Spiess, V., Blumenberg, M., Schneider, R.R., 2012. Gas
566 hydrate decomposition recorded by authigenic barite at pockmark sites of the northern
567 Congo Fan. Geo-Mar. Lett. 32, 515-524.

568 Laglera, L.M., van den Berg, C.M.G., 2009. Evidence for geochemical control of iron by
569 humic substances in seawater. Limnol. Oceanol. 54, 610-619.

570 Lamontagne, R.A. et al., 1973. Methane concentrations in various marine environments. J.
571 Geophys. Res. 78, 5317-5324.

572 Luff, R., Wallmann, K., 2003. Fluid flow, methane fluxes, carbonate precipitation and
573 biogeochemical turnover in gas hydrate-bearing sediments at Hydrate Ridge, Cascadia
574 Margin: Numerical modeling and mass balances. Geochim. Cosmochim. Acta 67, 3403-
575 3421.

576 Marcon, Y., Sahling, H., Allais, A.G., Bohrmann, G., Olu, K., 2014a. Distribution and
577 temporal variation of mega-fauna at the Regab pockmark (Northern Congo Fan), based
578 on a comparison of videomosaics and geographic information systems analyses. Mar.
579 Ecol., in press, doi:10.1111/maec.12056.

580 Marcon, Y., Ondreas, H., Sahling, H., Bohrmann, G., Olu, K., 2014b. Fluid flow regimes and
581 growth of a giant pockmark. Geology, in press, doi:10.1130/G34801.1.

582 Martens, C.S., Berner, R.A., 1974. Methane production in the interstitial waters of sulfate
583 depleted marine sediments. Science 185, 1167–1169.

584 Mastalerz, V., de Lange, G.J., Dahlmann, A., Feseker, T., 2007. Active venting at the Isis
585 mud volcano, offshore Egypt: Origin and migration of hydrocarbons. Chem. Geol. 246,
586 87-106.

587 McQuay, E.L., Torres, M.E., Collier, R.W., Huh, C.A., McManus, J., 2008. Contribution of
588 cold seep barite to the barium geochemical budget of a marginal basin. Deep-Sea Res. I
589 55, 801-811.

590 Millero, F.J., Sotolongo, S., Izaguirre, M., 1987. The oxidation kinetics of Fe(II) in seawater.
591 Geochim. Cosmochim. Acta 51, 793-801.

592 Millero, F.J., 1998. Solubility of Fe(III) in seawater. Earth Planet. Sci. Lett. 154, 323-329.

593 Misumi, K., Lindsay, K., Moore, J.K., Doney, S.C., Tsumune, D., Yoshida, Y., 2013. Humic
594 substances may control dissolved iron distributions in the global ocean: Implications
595 from numerical simulations. Global Biogeochem. Cycles 27, 450-462.

596 Noble, A.E., Lamborg, C.H., Ohnemus, D.C., Lam, P.J., Goepfert, T.J., Measures, C.I.,
597 Frame, C.H., Casciotti, K.L., DiTullio, G.R., Jennings, J., Saito, M.A., 2012. Basin-scale
598 inputs of cobalt, iron, and manganese from the Benguela-Angola front to the South
599 Atlantic Ocean. Limnol. Oceanol. 57, 989-1010.

600 Olu, K., Caprais, J.C., Galeron, J., Causse, R., von Cosel, R., Budzinski, H., Le Menach, K.,
601 Le Roux, C., Levache, D., Khripounoff, A., Sibuet, M., 2009. Influence of seep emission
602 on the non-symbiont-bearing fauna and vagrant species at an active giant pockmark in the
603 Gulf of Guinea (Congo-Angola margin). Deep-Sea Res. I 56, 2380-2393.

604 Olu-Le Roy, K., Caprais, J.C., Fifis, A., Fabri, M.C., Galéron, J., Budzinsky, H., Le Ménach,
605 K., Khripounoff, A., Ondréas, H., Sibuet, M., 2007. Cold-seep assemblages on a giant
606 pockmark off West Africa: spatial patterns and environmental control. Mar. Ecol. 28,
607 115-130.

608 Ondreas, H., Olu, K., Fouquet, Y., Charlou, J.L., Gay, A., Dennielou, B., Donval, J.P., Fifis,
609 A., Nadalig, T., Cochonat, P., Cauquil, E., Bourillet, J.F., Le Moigne, M., Sibuet, M.,
610 2005. ROV study of a giant pockmark on the Gabon continental margin. Geo-Mar. Lett.
611 25, 281-292.

612 Pierre, C., Fouquet, Y., 2007. Authigenic carbonates from methane seeps of the Congo deep-
613 sea fan. Geo-Mar. Lett. 27, 249-257.

614 Pierre, C. et al., 2012. Authigenic carbonates from active methane seeps offshore southwest
615 Africa. Geo-Mar Lett. 32, 501-513.

616 Ristova, P.P., Wenzhofer, F., Ramette, A., Zabel, M., Fischer, D., Kasten, S., Boetius, A.,
617 2012. Bacterial diversity and biogeochemistry of different chemosynthetic habitats of the
618 REGAB cold seep (West African margin, 3160 m water depth). Biogeosciences 9, 5031-
619 5048.

620 Riedinger, N., Kasten, S., Groger, J., Franke, C., Pfeifer, K., 2006. Active and buried
621 authigenic barite fronts in sediments from the Eastern Cape Basin. Earth Planet. Sci. Lett.
622 241, 876-887.

623 Rongemaille, E., Bayon, G., Pierre, C., Bollinger, C., Chu, N.C., Fouquet, Y., Riboulot, V.,
624 Voisset, M., 2011. Rare earth elements in cold seep carbonates from the Niger delta.
625 Chem. Geol. 286, 196-206.

626 Rousseau, T.C.C., Sonke, J.E., Chmeleff, J., Candaudap, F., Lacan, F., Boaventura, G.,
627 Seyler, P., Jeandel, C., 2013. Rare earth element analysis in natural waters by multiple
628 isotope dilution - sector field ICP-MS. J. Anal. Atom. Spectrom. 28, 573-584.

629 Rue, E.L., Bruland, K.W., 1995. Complexation of iron(III) by natural organic-ligands in the
630 Central North Pacific as determined by a new competitive ligand equilibration adsorptive
631 cathodic stripping voltammetric method. Mar. Chem. 50, 117-138.

632 Sahling, H., Bohrmann, G., Spiess, V., Bialas, J., Breitzke, M., Ivanov, M., Kasten, S.,
633 Krastel, S., Schneider, R., 2008. Pockmarks in the Northern Congo Fan area, SW Africa:
634 Complex seafloor features shaped by fluid flow. Mar. Geol. 249, 206-225.

635 Saito, M.A., Noble, A.E., Tagliabue, A., Goepfert, T.J., Lamborg, C.H., Jenkins, W.J., 2013.
636 Slow-spreading submarine ridges in the South Atlantic as a significant oceanic iron
637 source. Nat. Geosci. 6, 775-779.

638 Solomon, E. A., Kastner, M., MacDonald, I. R., Leifer, I. Considerable methane fluxes to the
639 atmosphere from hydrocarbon seeps in the Gulf of Mexico. Nat. Geosci. 2, 561-565
640 (2009).

641 Sander, S.G., Koschinsky, A., Massoth, G.J., Stott, M., Hunter, K.A., 2007. Organic
642 complexation of copper in deep-sea hydrothermal vent systems. Environ. Chem. 4, 81–89.

643 Sander, S.G., Koschinsky, A., 2011. Metal flux from hydrothermal vents increased by organic
644 complexation. Nat. Geosci. 4, 145-150.

645 Sarthou, G., Bucciarelli, E., Chever, F., Hansard, S.P., Gonzalez-Davila, M., Santana-
646 Casiano, J.M., Planchon, F., Speich, S., 2011. Fe(II) concentrations in the Atlantic sector
647 of the Southern Ocean along a transect from the subtropical domain to the Weddell Sea
648 Gyre. Biogeosciences 8, 2461–2479, doi:10.5194/bg-8-2461-2011.

649 Sauter, E.J., Muyakshin, S.I., Charlou, J.L., Schluter, M., Boetius, A., Jerosch, K., Damm, E.,
650 Foucher, J.P., Klages, M., 2006. Methane discharge from a deep-sea submarine mud
651 volcano into the upper water column by gas hydrate-coated methane bubbles. Earth
652 Planet. Sci. Lett. 243, 354-365.

653 Sherrell, R.M., Field, M.P., Ravizza, G., 1999. Uptake and fractionation of rare earth
654 elements on hydrothermal plume particles at 9 degrees 45 ' N, East Pacific Rise.
655 Geochim. Cosmochim. Acta 63, 1709-1722.

656 Sibuet, M., Olu, K. Biogeography, biodiversity and fluid dependence of deep-sea cold-seep
657 communities at active and passive margins. Deep-Sea Res. II 45, 517-567 (1998).

658 Statham, P.J., German, C.R., Connelly, D.P., 2005. Iron(II) distribution and oxidation
659 kinetics in hydrothermal plumes at the Kairei and Edmond vent sites, Indian Ocean .
660 Earth Planet. Sci. Lett. 236, 588-596.

661 Suess, E., 2010. Marine cold seeps. In: Handbook of hydrocarbon and lipid microbiology (Ed.
662 Timmis, K.N.). Springer, Berlin, pp. 188-203.

663 Tachikawa, K., Toyofuku, T., Basile-Doelsch, I., Delhaye, T., 2013. Microscale neodymium
664 distribution in sedimentary planktonic foraminiferal tests and associated mineral phases.
665 Geochim. Cosmochim. Acta 100, 11-23.

666 Tagliabue, A., Bopp, L., Dutay, J.C., Bowie, A.R., Chever, F., Jean-Baptiste, P., Bucciarelli,
667 E., Lannuzel, D., Remenyi, T., Sarthou, G., Aumont, O., Gehlen, M., Jeandel, C., 2010.
668 Hydrothermal contribution to the oceanic dissolved iron inventory. Nat. Geosci. 3, 252-
669 256.

670 Toner, B.M., Fakra, S.C., Manganini, S.J., Santelli, C.M., Marcus, M.A., Moffett, J., Rouxel,
671 O., German, C.R., Edwards, K.J., 2009. Preservation of iron(II) by carbon-rich matrices
672 in a hydrothermal plume. Nat. Geosci. 2, 197-201.

673 Toner, B.M., Marcus, M.A., Edwards, K.J., Rouxel, O., German, C.R., 2012. Measuring the
674 form of iron in hydrothermal plume particles. Oceanography 25, 209-212.

675 Torres, M.E., McManus, J., Huh, C.A., 2002. Fluid seepage along the San Clemente Fault
676 scarp: basin-wide impact on barium cycling. Earth Planet. Sci. Lett. 203, 181–194.

677 Vangriesheim, A., Khripounoff, A., Crassous, P., 2009. Turbidity events observed in situ
678 along the Congo submarine channel. Deep-Sea Res. II 56, 2208-2222.

679 Wallmann, K., Aloisi, G., Haeckel, M., Tishchenko, P., Pavlova, G., Greinert, J., Kutterolf,
680 S., Eisenhauer, A., 2008. Silicate weathering in anoxic marine sediments. Geochim.
681 Cosmochim. Acta 72, 2895-2918.

682 Wang, H., Yang, Q.H., Ji, F.W., Lilley, M.D., Zhou, H.Y., 2012. The geochemical
683 characteristics and Fe(II) oxidation kinetics of hydrothermal plumes at the Southwest
684 Indian Ridge. Mar. Chem. 134, 29-35.

685 Westbrook, G.K., et al., 2009. Escape of methane gas from the seabed along the West
686 Spitsbergen continental margin. Geophys. Res. Lett. 36, L15608,
687 doi:10.1029/2009GL039191.

688 Wu, J.F., 2007. Determination of picomolar iron in seawater by double Mg(OH)(2)
689 precipitation isotope dilution high-resolution ICPMS. Mar. Chem. 103, 370-381.

690 Yücel, M., Gartman, A., Chan, C.S., Luther III, G.S., 2011. Hydrothermal vents as a
691 kinetically stable source of iron-sulphide-nearing nanoparticles to the ocean. Nat. Geosci.
692 4, 367-371.

693

694

695 **Figure captions**

696 **Figure 1:** Location of the Regab and Baboon pockmarks in the Gulf of Guinea. Regab is
697 situated in close proximity to the Congo submarine canyon.

698 **Figure 2:** Microbathymetric map of the Regab pockmark showing the location of studied
699 sites and the distribution of seafloor habitats and carbonate-paved areas, as inferred from
700 ROV observations during the WACS cruise (2011). The distribution of methane
701 concentrations in bottom waters (+1-2 m above the seafloor) determined during the ZAI-ROV
702 project (2000) is also shown for comparison (Charlou et al., 2004).

703 **Figure 3:** Seafloor bottom photographs of typical seafloor habitats at Regab. A) Mussel
704 (*Mytilidae*) beds associated with massive carbonate pavements and seafloor gas hydrate
705 deposits in the central part of Regab. B) Details of a mussel field. C) *Vesicomyidae* field
706 (Clams). D) Methane venting at the Bubble site in the central part of Regab. E) Bushes of
707 vestimentiferan tubeworms (*Escarpia southwardae*) associated with hard carbonate
708 substrates. F) Seawater sampling (PEPS system) over microbial mats in the southeastern part
709 of the pockmark.

710 **Figure 4:** Depth profiles for total dissolvable (TD) and dissolved (DISS) concentrations of
711 Fe, Mn and Nd in unfiltered and filtered seawater samples, respectively.

712 **Figure 5:** Shale-normalized (PAAS) REE patterns for unfiltered and filtered seawater
713 samples at the Reference site, and at the Regab (Bubble site and seafloor habitat patches) and
714 Baboon pockmarks. Symbols: unfiltered samples (red circles); filtered samples (white
715 circles). The thick blue line represents the mean shale-normalized REE pattern for the water
716 column at the Reference site (except sample + 1m).

717 **Figure 6:** Total dissolvable (TD) Nd *versus* TDFe concentrations at the Congo seeps.
718 Symbols: Reference and East Pockmark sites (large white diamonds); Bubble site (red
719 squares); seafloor habitat patches (small orange diamonds); Baboon (green triangles). Values
720 for unfiltered seawater samples collected at methane seeps from the Niger Delta margin are
721 shown for comparison (black circles; Bayon et al., 2011a). The trends inferred from our data
722 would be controlled by the presence of Fe-Mn oxyhydroxide phases and easily leachable
723 sulfide minerals in the plume particles.

724 **Figure 7**: Relationships between methane and dissolved iron (Fe_{DISS}) and manganese
725 (Mn_{DISS}) concentrations in near-seafloor seawater samples at the Congo seeps. The legend for
726 symbols is given in the Fig. 6 caption.

Figure1
Click here to download Figure: Fig1.pdf

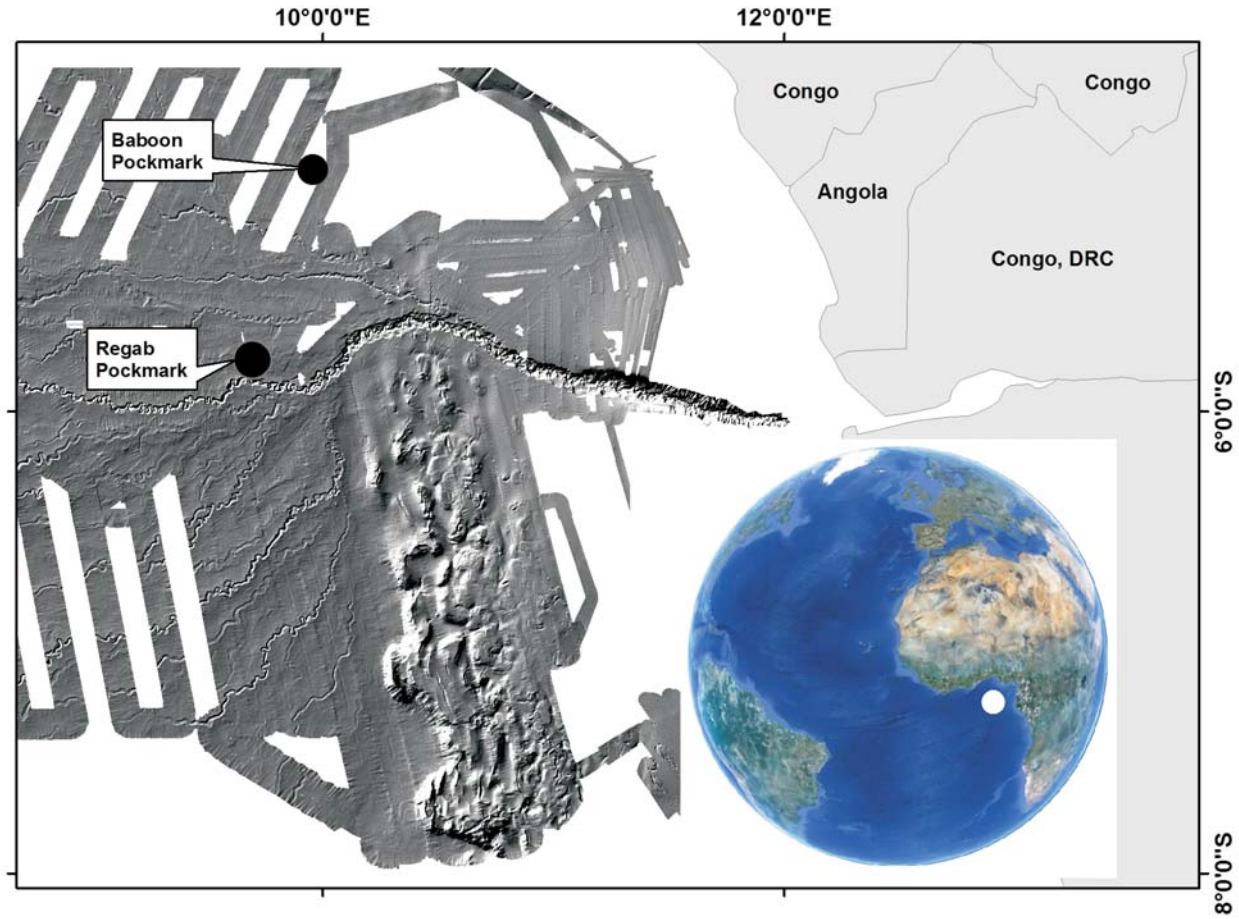

Fig. 1

Figure2
Click here to download Figure: Fig2.pdf

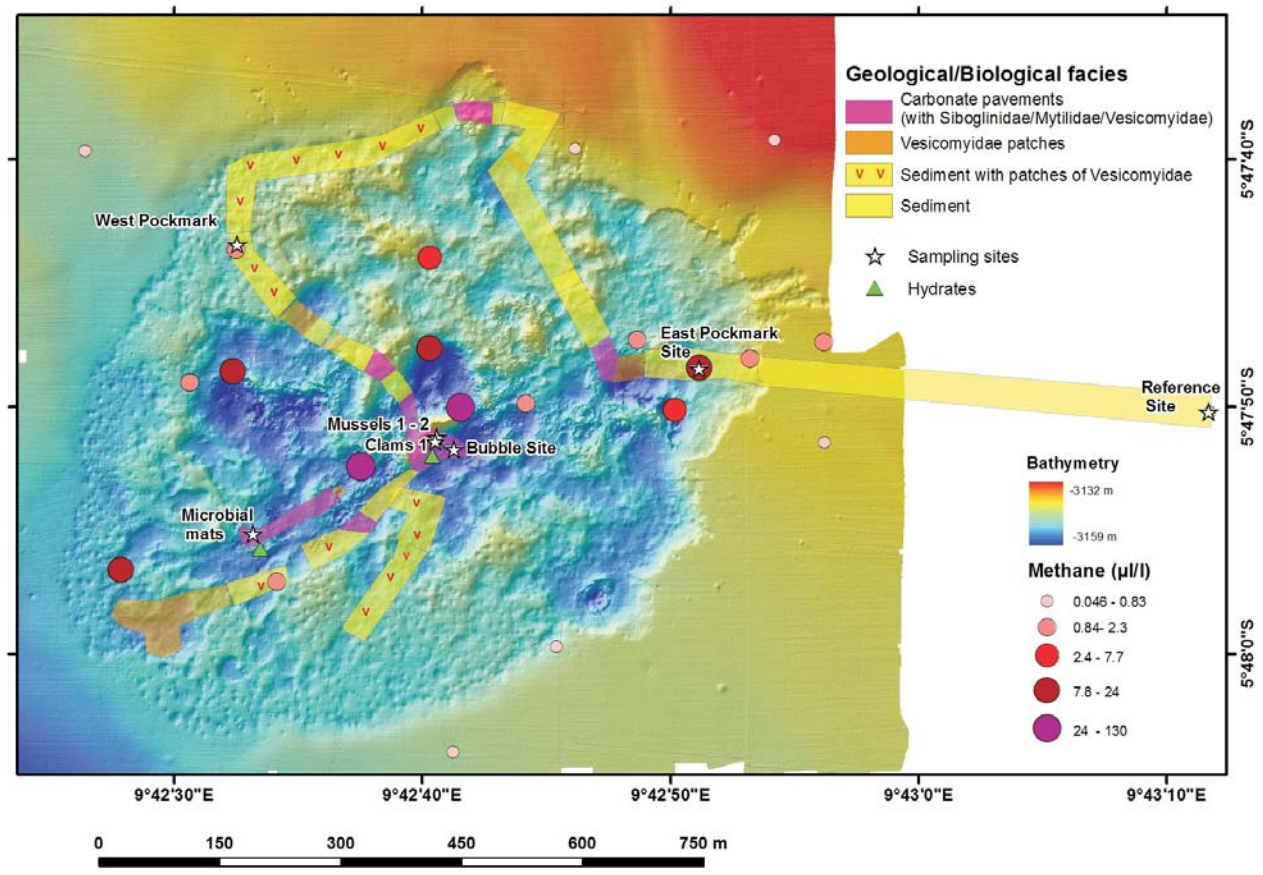

Fig. 2

Figure3
Click here to download Figure: Fig3.pdf

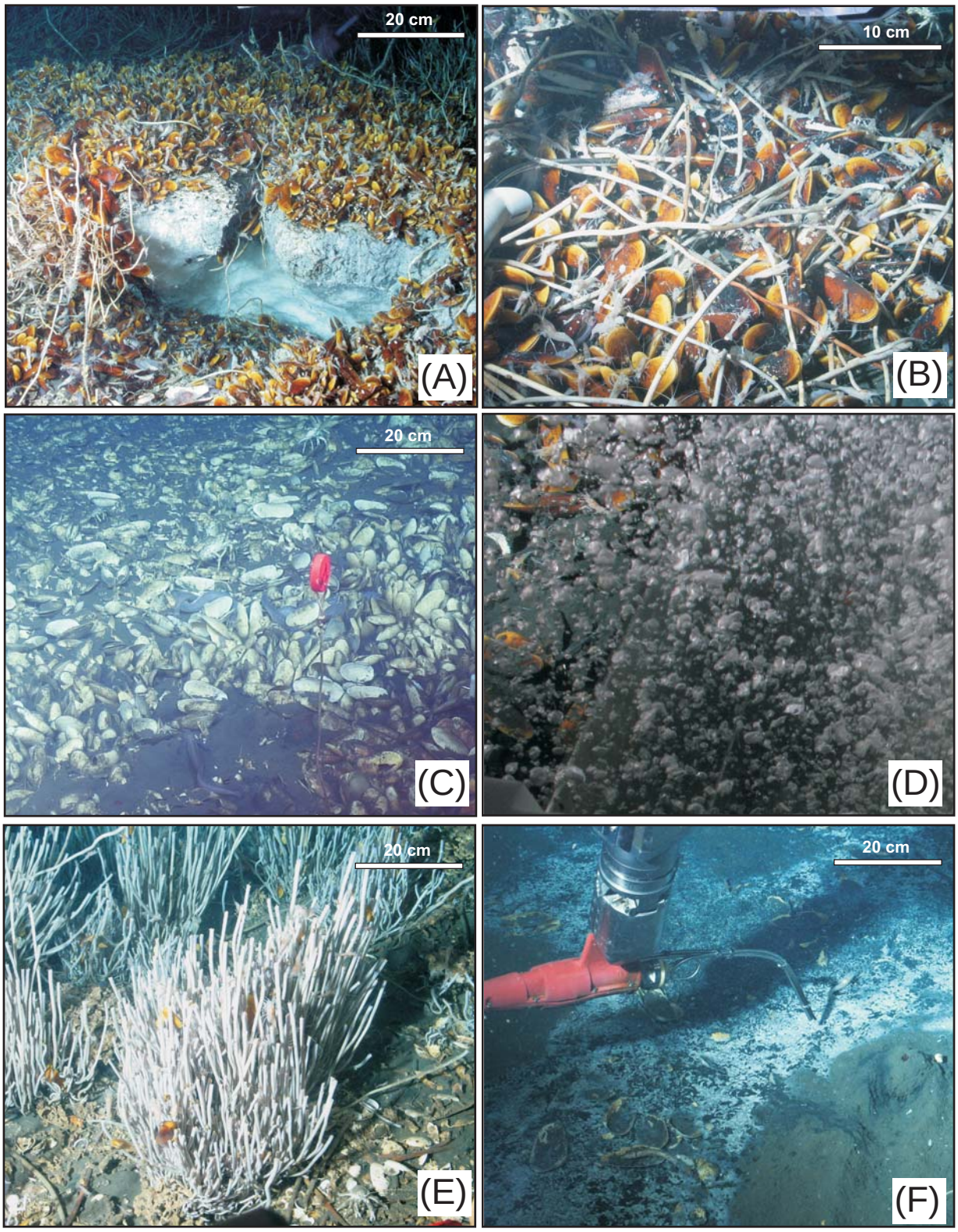

Fig. 3

Figure4

Click here to download Figure: Fig4.pdf

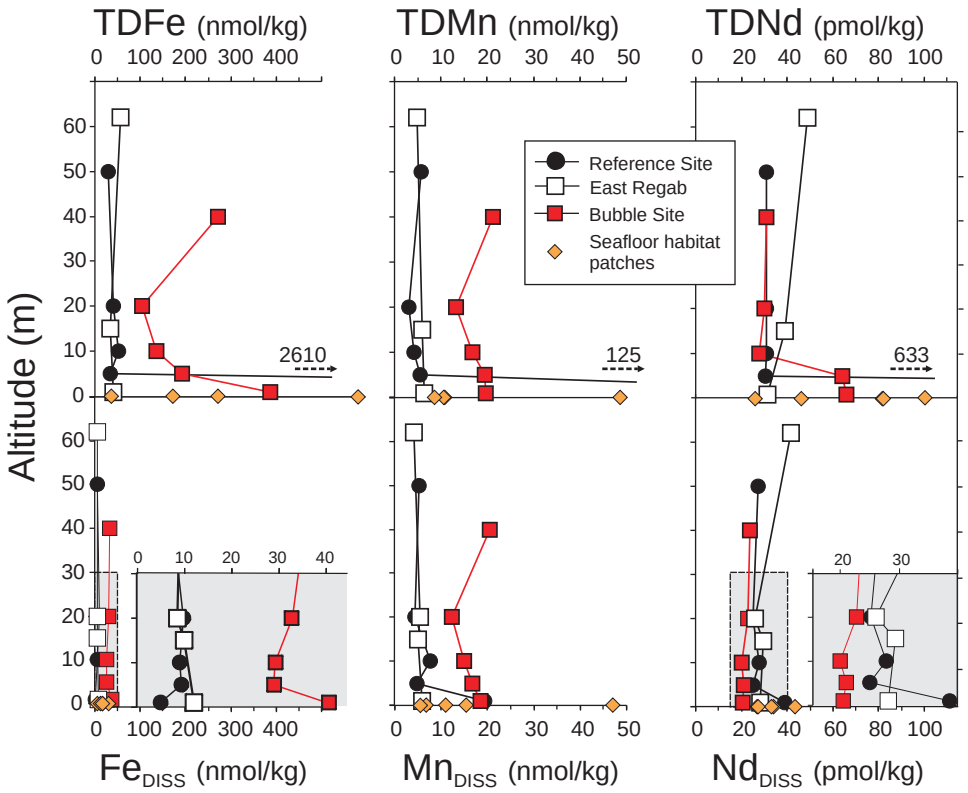

Fig. 4

Figure5
Click here to download Figure: Fig5.pdf

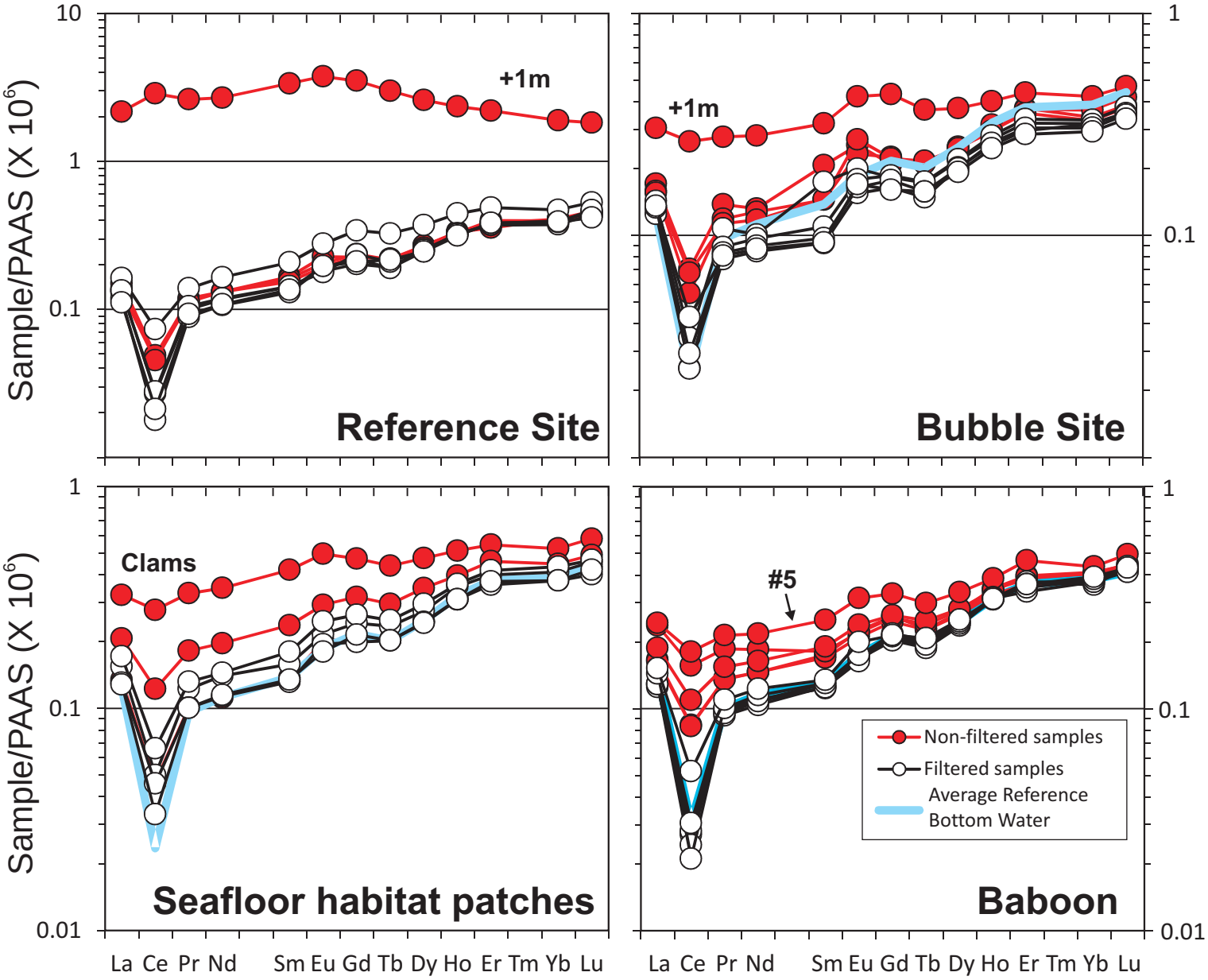

Fig. 5

Figure6
Click here to download Figure: Fig6.pdf

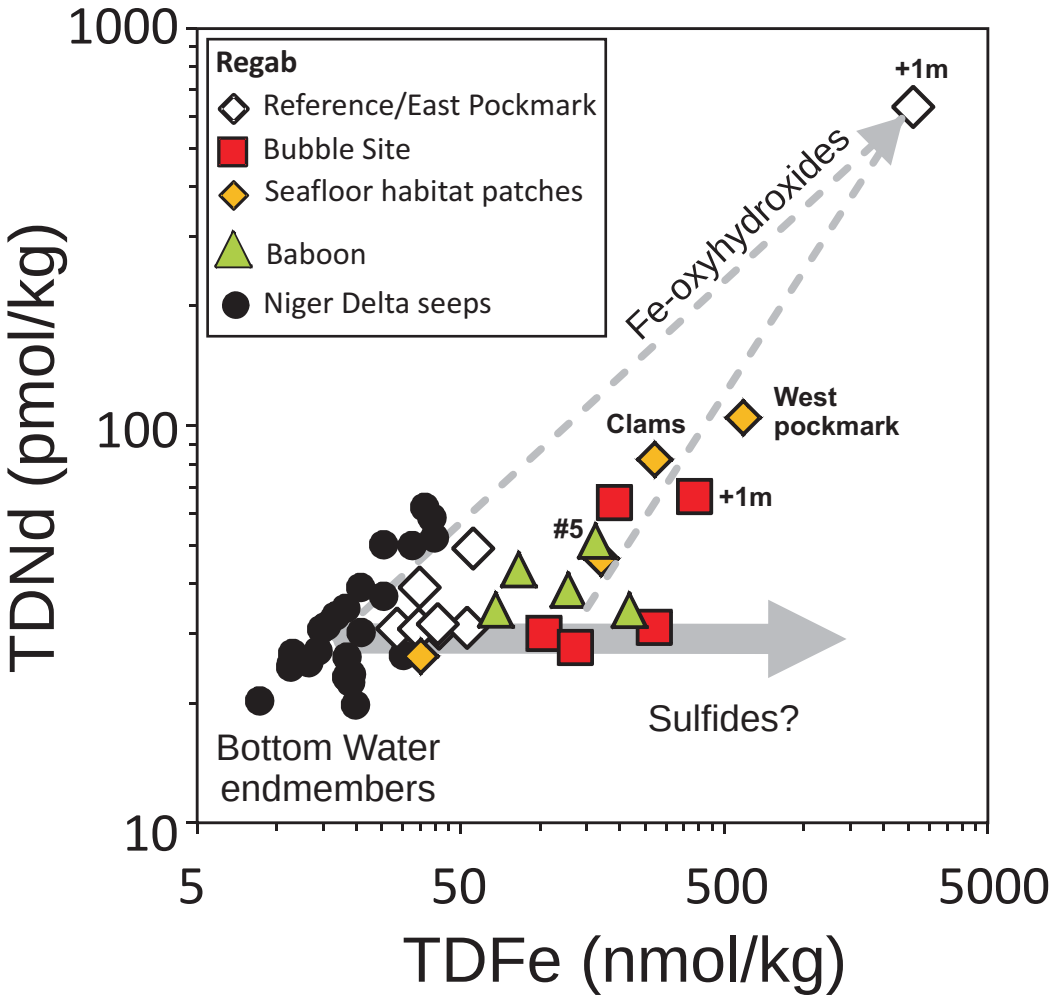

Fig. 6

Figure7
Click here to download Figure: Fig7.pdf

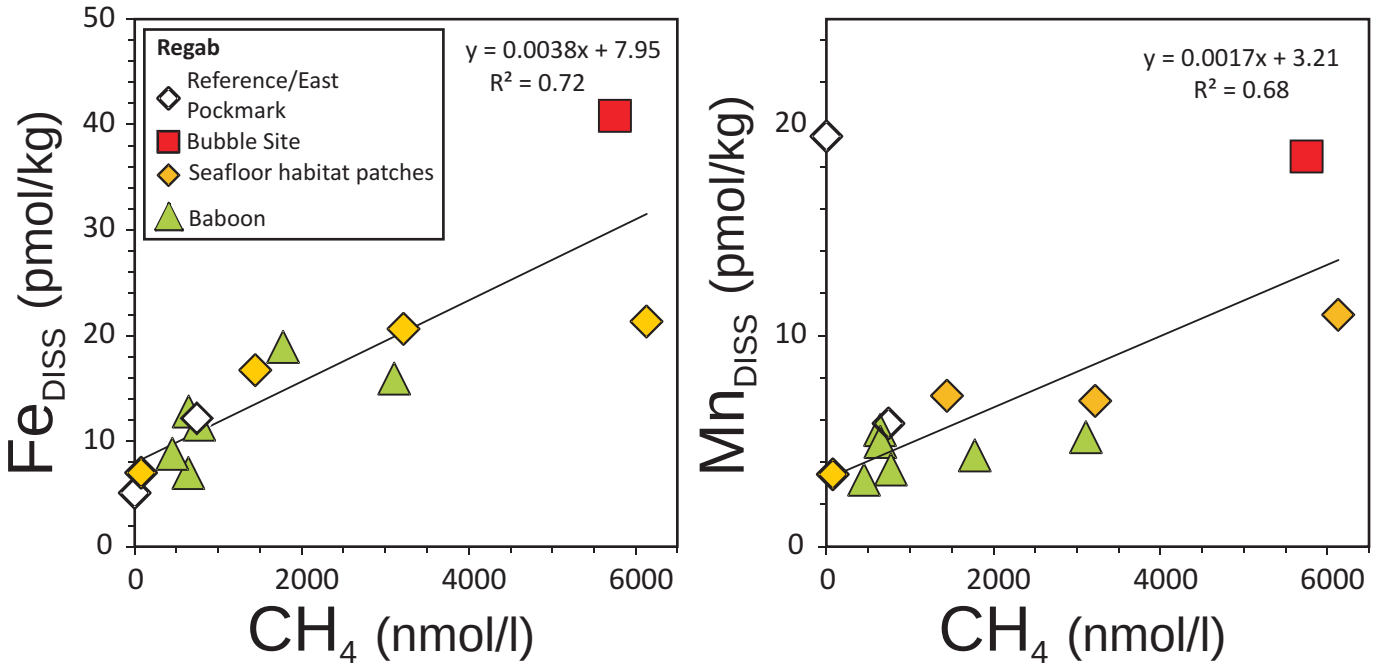

Fig. 7

Table1
Click here to download Table: Table1.pdf

Table 1
Locations of studied sampling sites at Regab and Baboon pockmarks

Sampling site	ROV Dive	Latitude	Longitude	Water depth
REGAB				
Reference Site	#429	S 5°47,837	E 9°43,195	3145 m
Bubble Site	#424	S 5°47,862	E 9°42,688	3156 m
East Pockmark Site	#429	S 5°47,808	E 9°42,852	3150 m
Seafloor chemosynthetic habitats				
West pockmark	#429			
Mytilidae field (Mussels)				
Mussel 1	#424	S 5°47,854	E 9°42,676	3152 m
Mussel 2	#425	S 5°47,853	E 9°42,675	3150 m
Vesicomyidae field (Clams)	#425	S 5°47,857	E 9°42,675	3154 m
Microbial mats	#427	S 5°47,919	E 9°42,553	3153 m
BABOON				
#1	#432	S 4°56,601	E 9°57,338	3047 m
#2	#432	S 4°56,432	E 9°57,088	3040 m
#3	#432	S 4°56,296	E 9°56,984	3035 m
#4	#432	S 4°56,238	E 9°56,988	3042 m
#5	#432	S 4°56,195	E 9°56,975	3046 m
#6	#432	S 4°56,203	E 9°56,961	3047 m

Table2

Click here to download Table: Table2.pdf

Table 2

Trace element concentrations of non-filtered seawater samples at Regab and Baboon pockmarks.

	Mn (nmol kg^{-1})	Fe	Y (pmol kg^{-1})	La	Ce (pmol kg^{-1})	Pr	Nd (pmol kg^{-1})	Sm	Eu (pmol kg^{-1})	Gd	Tb (pmol kg^{-1})	Dy	Ho (pmol kg^{-1})	Er	Yb (pmol kg^{-1})	Lu
REGAB																
Reference Site																
50 m	5.7	29	180	41	28	7.2	31	6.0	1.45	7.0	1.05	7.8	1.97	6.8	6.5	1.09
20 m	3.0	41	151	36	26	7.0	31	5.7	1.37	6.8	1.06	7.5	2.00	6.1	6.7	1.07
10 m	4.1	53	157	38	26	7.4	31	6.1	1.61	6.7	1.07	7.7	2.00	6.5	6.6	1.14
5 m	5.4	35	162	36	20	7.2	31	5.9	1.57	7.0	1.06	7.6	1.99	6.4	6.3	1.14
1 m	125	2610	662	595	1632	164	633	124	27	104	14.6	75	14.1	37	31	4.5
Bubble Site																
40 m	21	272	187	47	40	8.6	31	7.6	1.81	6.2	1.03	7.2	1.76	6.4	5.6	0.95
20 m	13	104	197	44	31	7.4	30	5.3	1.66	6.7	1.02	7.2	1.89	6.3	6.0	1.04
10 m	17	137	192	43	38	7.1	28	5.4	1.92	6.6	1.05	7.1	1.78	6.0	5.4	0.93
5 m	19	192	204	135	182	21	64	6.1	1.83	7.9	1.13	7.7	1.89	6.0	5.8	0.97
1 m	20	386	221	84	150	17	66	11.8	3.00	12.8	1.79	10.8	2.42	7.5	6.9	1.16
East Pockmark Site																
62 m	4.8	56	213	66	95	12.8	49	9.0	2.16	9.8	1.48	9.5	2.33	7.4	6.8	1.13
15 m	6.1	35	232	48	27	8.9	39	7.4	1.98	9.1	1.35	9.5	2.60	8.0	8.3	1.31
1 m	6.3	41	169	41	30	7.6	32	5.9	1.58	7.2	1.08	7.3	1.89	5.9	5.9	1.01
Seafloor chemosynthetic habitats																
West Pockmark																
1 m	6.7	592	228	110	173	26.1	104	19.9	4.22	19.5	2.83	14.8	3.60	9.4	9.1	1.45
Mytilidae field (Mussels)																
#1 (0.1 m)	49	35	186	37	26	6.4	26	5.1	1.43	6.1	0.99	7.1	1.86	6.3	6.4	1.08
#2 (0.1 m)	8.6	171	221	57	70	11.4	46	8.7	2.08	9.4	1.44	10.0	2.38	7.8	7.3	1.21
Vesicomyidae field (Clams)																
0.1 m	10.7	273	230	89	158	21	82	16	3.53	14.0	2.14	13.7	3.08	9.3	8.6	1.44
BABOON																
#1 (3 m)	6.7	219	196	46	48	8.6	34	6.5	1.60	7.7	1.11	7.8	2.06	6.5	6.6	1.06
#2 (3 m)	5.3	68	195	45	47	8.5	34	6.3	1.49	7.3	1.10	7.6	1.97	6.2	6.1	1.07
#3 (3 m)	4.8	83	204	65	89	11.7	43	6.7	1.57	7.6	1.17	8.0	2.09	6.8	6.7	1.10
#4 (3 m)	4.3	128	203	52	62	9.7	38	7.0	1.70	7.8	1.21	8.1	2.05	6.7	6.6	1.11
#5 (3 m)	4.0	163	215	67	103	13.4	51	9.3	2.24	9.8	1.45	9.6	2.32	7.9	7.1	1.23
#6 (3 m)	6.8	287	-	-	-	-	-	-	-	-	-	-	-	-	-	-

Table3

Click here to download Table: Table3.pdf

Table 3

Trace element concentrations of filtered seawater samples at Regab and Baboon pockmarks.

Altitude (m)	Mn (nmol kg^{-1})	Fe (pmol kg^{-1})	Y (pmol kg^{-1})	La (pmol kg^{-1})	Ce (pmol kg^{-1})	Pr (pmol kg^{-1})	Nd (pmol kg^{-1})	Sm (pmol kg^{-1})	Eu (pmol kg^{-1})	Gd (pmol kg^{-1})	Tb (pmol kg^{-1})	Dy (pmol kg^{-1})	Ho (pmol kg^{-1})	Er (pmol kg^{-1})	Yb (pmol kg^{-1})	Lu (pmol kg^{-1})
Reference Site																
50 m	5.3	8.0	175	37	15	6.3	27	5.2	1.28	6.0	0.94	7.3	1.92	6.4	6.5	1.11
20 m	5.6	10.0	153	31	12	5.8	25	5.0	1.39	6.2	1.05	7.1	1.89	6.5	6.4	1.03
10 m	7.7	9.2	166	37	16	6.6	28	5.3	1.27	7.0	1.02	7.2	1.93	6.4	6.3	1.16
5 m	7.0	9.5	164	32	10	5.6	25	4.8	1.37	6.5	0.92	7.1	1.96	6.3	6.1	1.07
1 m	19	5.1	196	45	42	8.7	39	7.7	1.97	10.1	1.58	10.6	2.67	8.3	7.7	1.30
Bubble Site																
40 m	21	36	176	39	20	6.7	24	6.4	1.42	5.4	0.84	6.2	1.63	5.5	5.2	0.88
20 m	12	33	184	37	14	5.6	23	4.0	1.27	5.5	0.85	6.3	1.69	5.7	5.4	0.94
10 m	15	30	180	34	14	4.9	20	3.4	1.10	4.9	0.72	5.8	1.53	5.1	5.2	0.88
5 m	17	29	182	37	17	5.2	21	3.6	1.17	5.2	0.77	5.8	1.57	5.2	5.0	0.86
1 m	18	41	173	37	24	5.1	20	3.4	1.21	4.8	0.77	5.6	1.48	4.9	4.8	0.83
East Pockmark Site																
62 m	4.2	8.5	209	55	65	10.4	42	7.7	1.87	8.6	1.25	8.7	2.18	6.8	6.6	1.10
20 m	5.5	8.7	200	39	18	6.4	26	4.8	1.25	6.5	0.97	7.4	1.86	5.7	6.0	0.99
15 m	5.0	10.1	207	39	12	7.4	29	5.4	1.46	7.5	1.24	8.4	2.14	7.0	7.5	1.25
1 m	5.8	12.2	167	38	20	6.8	28	5.5	1.20	7.1	0.98	6.8	1.71	5.9	5.7	0.96
Seafloor chemosynthetic habitats																
West Pockmark																
1 m	4.4	7.0	165	34	15	6.3	26	4.8	1.25	6.3	1.04	6.8	1.80	6.2	5.8	1.04
Mytilidae field (Mussels)																
#1 (0.1 m)	47	34	180	36	26	6.3	27	4.9	1.38	5.9	0.98	7.1	1.86	6.1	6.1	0.99
#2 (0.1 m)	6.9	21	180	35	19	6.3	27	5.0	1.28	6.4	0.99	7.0	1.86	6.4	6.1	1.04
Vesicomyidae field (Clams)																
0.1 m	11.0	21	201	47	37	8.3	34	6.6	1.75	7.8	1.22	8.5	2.18	7.1	7.1	1.15
Microbial mats																
0.1 m	7.1	17	188	43	28	7.7	33	5.8	1.53	7.2	1.14	7.9	2.12	6.8	6.7	1.13
BABOON																
#1 (3 m)	5.5	7.0	195	36	15	6.1	26	4.8	1.24	6.1	0.93	7.0	1.86	6.3	5.9	1.07
#2 (3 m)	5.0	12.8	182	34	16	5.8	24	4.6	1.19	6.0	0.91	6.8	1.89	5.7	6.1	1.02
#3 (3 m)	4.3	18.9	196	35	14	6.3	26	4.6	1.23	6.5	0.99	7.0	1.91	6.0	6.2	1.05
#4 (3 m)	3.7	11.6	194	35	12	6.0	25	4.6	1.16	6.3	0.98	6.9	1.87	6.4	6.1	1.08
#5 (3 m)	3.2	8.8	194	40	17	6.3	27	4.8	1.24	6.3	0.94	7.1	1.89	6.2	6.2	1.02
#6 (3 m)	5.2	15.9	196	42	30	6.9	29	5.0	1.42	6.3	1.01	7.2	1.87	6.2	6.4	1.07

TableS1

Click here to download Table: TableS1.pdf

Table S1

Trace element concentrations of certified reference materials used in this study.

	Mn (µg kg^{-1})	Fe (µg kg^{-1})	Y (ng kg^{-1})	La (ng kg^{-1})	Ce (ng kg^{-1})	Pr (ng kg^{-1})	Nd (ng kg^{-1})	Sm (ng kg^{-1})	Eu (ng kg^{-1})	Gd (ng kg^{-1})	Tb (ng kg^{-1})	Dy (ng kg^{-1})	Ho (ng kg^{-1})	Er (ng kg^{-1})	Yb (ng kg^{-1})	Lu (ng kg^{-1})
NASS-6 (n=11)																
mean	0.50	0.48	23.1	9.87	3.64	1.50	6.40	1.13	0.24	1.51	0.22	1.61	0.42	1.35	1.30	0.22
s	0.09	0.07	2.7	0.89	0.54	0.10	0.26	0.05	0.01	0.08	0.01	0.07	0.02	0.03	0.06	0.01
certified	0.52	0.48														
deviation (%)	-3.4	0.2														
RSD (%)	18.9	15.6	11.7	9.1	14.7	6.4	4.1	4.1	3.6	5.4	3.4	4.1	4.4	2.4	4.3	5.6
CASS-5 (n=12)																
mean	2.41	1.44	20.1	7.94	3.44	1.17	5.02	1.24	0.20	1.29	0.18	1.31	0.34	1.12	1.09	0.18
s	0.41	0.02	2.6	0.85	0.55	0.09	0.23	0.05	0.01	0.06	0.01	0.07	0.01	0.03	0.02	0.01
certified	2.56	1.4		7.95	3.36	1.16	5.02	1.22	0.2	1.21	0.17	1.23	0.32	1.07	1.08	0.19
deviation (%)	-6.4	3.1		-0.1	2.3	1.0	0.0	2.3	-1.3	6.4	3.0	6.3	8.6	5.1	0.6	-2.3
RSD (%)	16.9	1.4	12.9	10.6	16.0	7.3	4.7	3.8	4.6	5.0	4.0	5.3	3.0	3.0	2.0	3.5
In-house seawater standard - Concarneau Bay (n=4)																
mean	0.04	0.15	17.1	1.98	1.54	0.63	3.10	0.74	0.21	1.24	0.20	1.39	0.35	1.13	1.08	0.17
s	0.01	0.05	1.9	0.25	0.38	0.04	0.12	0.04	0.01	0.10	0.01	0.07	0.02	0.03	0.01	0.00
certified																
deviation (%)																
RSD (%)	29.6	33.5	11.1	12.5	24.4	5.8	3.9	5.5	4.3	8.3	5.1	5.1	6.0	2.7	0.2	0.7

TableS2

Click here to download Table: TableS2.pdf

Table S2

Methane, Fe_{DISS} and Mn_{DISS} concentrations at the Congo seeps

Sampling site	Altitude (m)	CH_4 (µl/l)	CH_4 (nmol/l)	Mn_{DISS} (nmol/kg)	Fe_{DISS} (nmol/kg)
REGAB					
Reference Site	+1m	0.046[a]	2	19.4	5.1
Bubble Site	+1m	128.9[a]	5755	18.5	40.8
East Pockmark Site	+1m	16.7[a]	745	5.8	12.2
Seafloor chemosynthetic habitats					
West pockmark	+1m	1.8[a]	80	4.3	7.0
Mytilidae field (Mussel 2)	+0.1m	72.2[b]	3223	6.9	20.6
Vesicomyidae field (Clams)	+0.1m	137.4[b]	6134	11.0	21.3
Microbial mats	+0.1m	32.4[b]	1446	7.1	16.7
BABOON					
#1	+3m	14.5[b]	647	5.5	7.0
#2	+3m	14.6[b]	652	5.0	12.8
#3	+3m	39.9[b]	1781	4.3	18.9
#4	+3m	17.4[b]	777	3.7	11.6
#5	+3m	10.2[b]	455	3.2	8.8
#6	+3m	69.7[b]	3112	5.2	15.9

[a] Charlou et al. (2004); [b] This study